Cao, T., Cryan, M. J., Ho, Y-L. D., Craddock, I. J., & Railton, C. J. (2007). Fast-light based pulse compression in 2-D photonic crystal waveguides. IEEE Journal of Lightwave Technology, 25(9), 2590 - 2598. 10.1109/JLT.2007.903825

Fast-Light Based Pulse Compression in 2-D Photonic Crystal Waveguides

Tun Cao, Martin J. Cryan, *Senior Member, IEEE*, Ying-Lung Daniel Ho, Ian J. Craddock, and Chris J. Railton

***Abstract*—Chirped-pulse propagation close to a mini-stopband (MSB) in short photonic crystal (PhC) waveguides is studied using the 2-D finite-difference time-domain method. The group delay (GD) is calculated for different length waveguides and is shown to have a nonlinear relationship with length, implying that dispersion diagram based design approaches may not be applicable in these cases. Pulse compression is then observed directly in the time domain, and a GD-based analysis is used to explain the results. It is shown that the fast-light or negative GD region that is found within the MSB plays a more important role than pulse filtering effects, which can also induce compression. The GD analysis is then used to find the optimum length waveguide for the maximum pulse compression, and this is found to be in agreement with direct time-domain results. Finally, a different PhC waveguide structure is studied based on square holes, which results in an increased GD and, hence, increased pulse compression.**

***Index Terms*—Photonic crystals (PhCs), pulse compression, waveguide dispersion.**

I. Introduction

THERE has been much interest in the use of photonic crystal (PhC) waveguides in pulse compression applications [1]–[5]. It has become clear, however, that it is difficult for these waveguides to produce the large amounts of corrective dispersion that are required in long-haul telecommunications systems. Research has thus focused on applications where the twin advantages of PhCs of very small size and the potential for tunability are important. One example could be the fine tuning of the overall dispersion that is used within a receiver photonic integrated circuit or the possible direct integration of a dispersive element within a laser or semiconductor optical amplifier (SOA) [6] to correct or even prechirp device output pulses. In these applications, it is important to understand how to generate the required amount of dispersion and what might be the optimum length of a PhC waveguide. A typical approach to this problem would be to calculate the dispersion diagram for the PhC waveguide and to calculate the group velocity, and hence the group velocity dispersion (GVD), from these data. While this approach works well in general, there are cases, such as when operating near to a mini-stopband (MSB) with short-length waveguides, that it begins to break down. In particular, near an MSB, mode coupling occurs, leading to back reflection. As is well known in this regime, transmittance and phase shift no longer have simple relationships with device length. The following equations show these relationships for weak 1-D gratings [7], [8]:

$$T = 1 - \tanh^2(\kappa L) \tag{1}$$

$$\phi = \arctan\left(\frac{\delta}{\Omega}\tanh(\Omega L)\right) \tag{2}$$

where T is the transmittance, κ is the coupling coefficient, δ is the frequency detuning factor, L is the device length, and $\Omega = \sqrt{\kappa^2 - \delta^2}$. This simple theory has been extended to the more complex case of PhC waveguide MSBs [9], and this has been used to extract the loss parameters for these waveguides. This paper investigates, for what is believed to be the first time, the phase shift and, hence, the group delay (GD) relationship with the length for these waveguides. This then enables the effect of the waveguides on propagating pulses to be analyzed in detail, and predictions are made as to the pulse compression or expansion that can occur. The GD is also used to understand the mechanism of pulse compression in MSBs, and the well-known "fast-light" [10] or negative GD region that is found within the MSB is found to play a major role in the effect. Finally, an attempt is made to maximize the pulse compression in a given length of waveguide; it is found that square-hole-based PhC waveguides can produce a narrower MSB and, hence, have an increased negative GD, which, in turn, leads to an increased pulse compression.

II. Modeling

This paper uses the 2-D finite-difference time-domain (FDTD) method to study the propagation of pulses in these waveguides [11], both directly in the time domain and via Fourier transforms in the frequency domain. A number of important features have been implemented in this in-house code, which allow a detailed study of pulse propagation. First, modal excitation and mode overlap integrals [12], [13] have been implemented, which allow very accurate determination of the phase shift through the device. Second, linearly chirped pulses can be defined, which is a necessary requirement to observe pulse compression in any linear system. The following equation

Manuscript received January 15, 2007; revised June 25, 2007. This work was supported by the Ultrafast Photonics Collaboration, U.K.

T. Cao was with the Photonics Research Group, Centre for Communications Research, Department of Electrical and Electronic Engineering, University of Bristol, BS8 1UB Bristol, U.K. He is now with the Detectors and Nuclear Science Research Group, Institute of Health Sciences, City University, Northampton Square, EC1V OHP London, U.K. (e-mail: tun.cao@bristol.ac.uk).

M. J. Cryan, Y.-L. D. Ho, I. J. Craddock, and C. J. Railton are with the Centre for Communications Research, Department of Electronic and Electrical Engineering, University of Bristol, BS8 1UB Bristol, U.K. (e-mail: m.cryan@bristol.ac.uk; Daniel.Ho@bristol.ac.uk; ian.craddock@bristol.ac.uk; Chris.Railton@bristol.ac.uk).

Color versions of one or more of the figures in this paper are available online at http://ieeexplore.ieee.org.

Digital Object Identifier 10.1109/JLT.2007.903825

shows the linearly chirped-pulse excitation of the electric field, E that has been used:

$$E(t) = \exp\left(-\frac{1}{2}\frac{(t-d)^2}{t_o^2}\right)\cos\left[\omega_o t - \left(\frac{1}{2}C\frac{(t-d)^2}{t_o^2}\right)\right] \tag{3}$$

where d is the time delay of the center of the pulse, ω_0 is the radial carrier frequency, t_0 is the half-width at $1/e$ intensity, and C is the chirp parameter. The expression shows that we have a Gaussian-shaped amplitude term multiplied by a carrier wave whose frequency varies with time. The C parameter describes how far the pulse is from being transformed limited. Thus, for a 900-fs wide pulse ($1/e$ intensity half-width), which will be used later in this paper, with a C parameter of ± 2, the transform-limited width is 402 fs.

The C parameter can be used in combination with the dispersion relation for the particular waveguide [14] to describe pulse dispersion. The dispersion relation is described in terms of $\omega-\beta$ diagrams, where β is the propagation constant. From these diagrams, the GVD can be calculated; this is the second derivative of β with respect to ω and is known as β_2. It can be shown that that for pulse compression to occur, the following relation must hold [14]:

$$\beta_2 C < 0. \tag{4}$$

Thus, β_2 and C must have opposite signs for compression to occur. However, an important point must be stressed here: The said assumption is only true when the higher order derivatives of the dispersion relation are assumed to be zero, i.e., $\beta_3 = \beta_4 = \cdots = 0$. For fiber-based systems, with typical pulsewidths greater than a few tens of picoseconds, this is a reasonable assumption; however, in the strong dispersion environment of PhC guides, this may not be true, and much more complex pulse behavior can occur, as outlined in [14]. This paper concentrates on ultrashort pulses with pulsewidths on the order of picoseconds, and their large spectral width increases the importance of higher order dispersion terms [14]. This paper, however, uses an alternative approach to dispersion diagrams for determining pulse behavior in linear systems based on GD. This approach is valid for any type of dispersion and automatically includes the effects of all higher order dispersive terms, which will be described in detail in Section III.

III. Results

Fig. 1 shows a top view of the structure to be studied. This is a narrowed W3 waveguide in the $\Gamma-K$ direction with a lattice constant of 480 nm. The narrowed W3 waveguide is reduced from an initial width of 1.66 μm ($= 2\sqrt{3} \times 480$ nm) to 1.34 μm; this is to place an MSB near to 1550 nm [15]. It should be noted that to align with the FDTD mesh, which is 10 $\times$ 10 nm in this case, the vertical spacing between rows has been adjusted from 415.69 nm ($= 480 \times \sqrt{3}/2$) to 420 nm. The waveguide is excited by the fundamental TE mode (E_x is the dominant field component) of the input photonic wire waveguide. This feature enables realistic excitation of the structure and allows overlap integrals to be performed at the

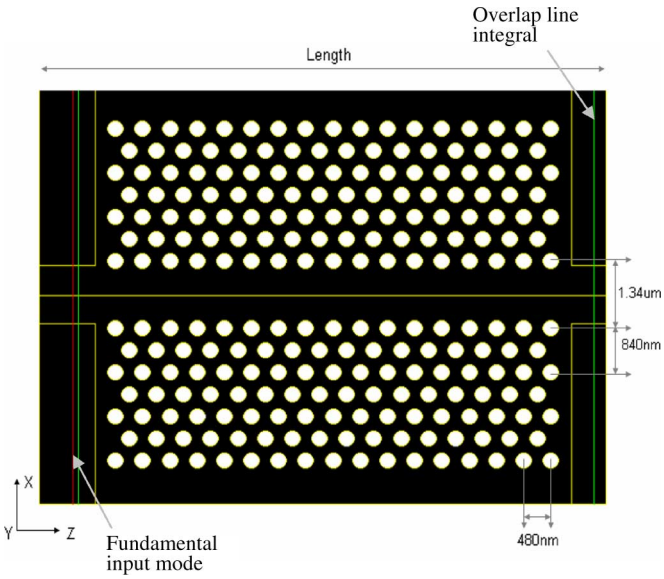

Fig. 1. FDTD model of a narrowed W3 PhC waveguide with $a = 480$ nm, $r/a = 0.329$, $\Gamma-K$ direction, $n = 3.24$, and length $= 5$, 10, 16, 20, 25, and 30 μm. The FDTD mesh size in the horizontal and vertical directions is 10 nm.

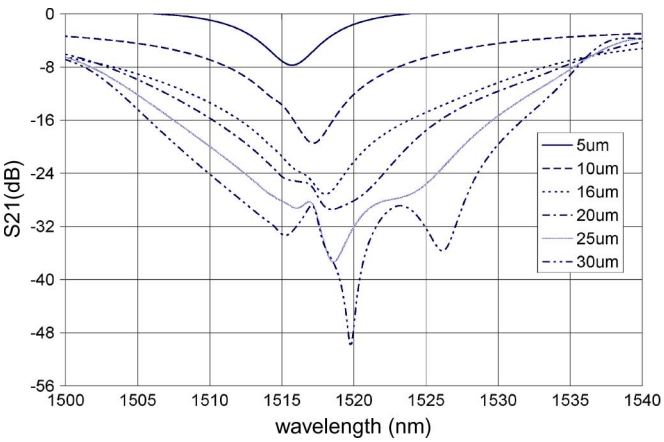

Fig. 2. FDTD simulated transmission for waveguide of Fig. 1 with lengths 5, 10, 16, 20, 25, and 30 μm.

output of the waveguide [12]. The transmission response of the structure is calculated by first performing a simulation with a simple straight waveguide and no PhC present in order to remove the effects of reflection from the PhC waveguide. After Fourier transforming the time-domain data, the frequency-domain Poynting vector gives the total input power. This procedure is repeated at the output of the guide with the PhC waveguide present. The ratio of these two powers gives the transmittance.

Fig. 2 shows the FDTD transmission for the different length waveguides, and the MSB is clearly observed. As expected, the depth of the MSB increases with increasing length; however, as the length increases, more complex behavior occurs within the MSB. As noted in [9], in the case of MSBs, unlike simple 1-D gratings, the bandwidth increases with increasing length due to the highly lossy nature of the higher order mode into which the fundamental mode is coupling. Another feature of these results is the fact that the center of the MSB is shifting

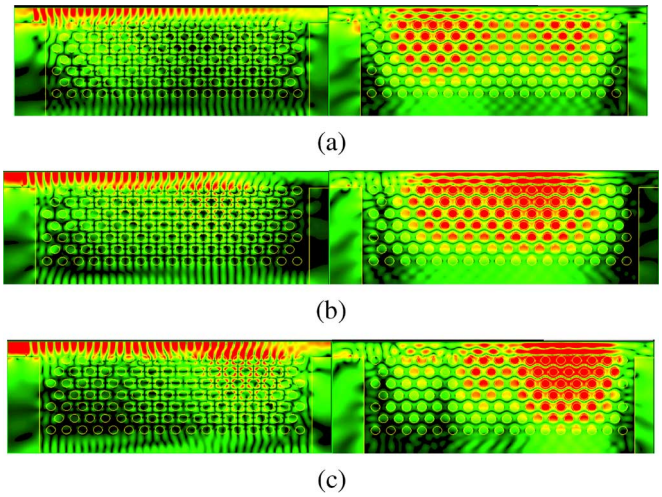

Fig. 3. Magnitude of (left) E_x and (right) E_z at different wavelengths across the MSB for the round-hole PhC waveguide. (a) 1511 nm. (b) 1517 nm. (c) 1523 nm. Dark gray: high field; light gray: low field.

to longer wavelengths with increasing length. It is not clear at this stage whether this is a numerical dispersion-related effect [11] or a real effect that is observed in these short lengths, where idealized Bloch mode transmission may not be realized. Detailed study of this will be the subject of future work.

The different length results can be used in conjunction with (1) to determine an effective 1-D coupling coefficient for the structure, and a value of 0.225 μm^{-1} is obtained. This is similar to the value of 0.28 μm^{-1}, which is obtained using a more accurate approach [9] for a similar structure.

One of the powerful features of the FDTD method is that all the fields in the device can be viewed at any wavelength through the use of Fourier transforms. Fig. 3 shows the so-called frequency-domain snapshots of the electric fields within the 10-μm-long device. These are obtained from running Fourier transforms that are performed within the simulation. The left column shows the magnitude of the E_x components, and the right column shows the E_z components. These results illustrate very well the strong mode coupling that occurs inside the MSB. The multiple intensity peaks in the z component are characteristic of higher order modes, and the reduction in intensity at 1517 nm, in the center of the MSB, is also evident. It can also be seen that the MSB is not symmetrical in terms of its upper and lower edges, and this will have a small influence on the pulse compression behavior at the two edges. The results also show evidence for beating effects, which could be influencing the phase response of the device.

Having calculated the transmission through the structure using Fourier transforms, the phase response of the device can also be calculated. The GD, τ_g is then calculated using

$$\tau_g = -\frac{d\phi}{d\omega} \tag{5}$$

where ϕ is the phase of the transmission coefficient, and ω is the radial carrier frequency.

Figs. 4 and 5 show the results for the different length guides, and the characteristic negative GD or fast-light region associated with these grating-like structures can be seen [16],

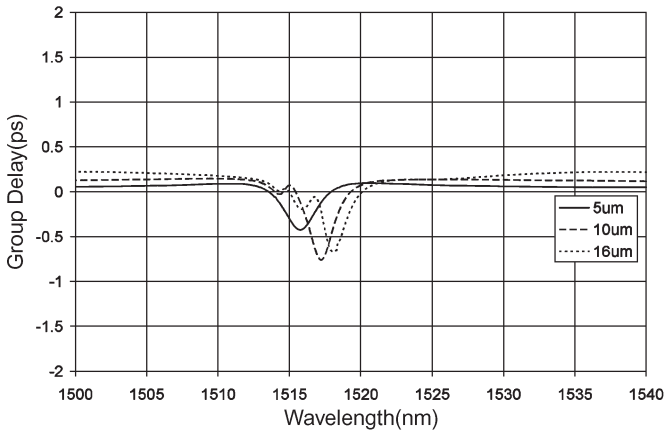

Fig. 4. GD of MSB for 5-, 10-, and 16-μm-long waveguides.

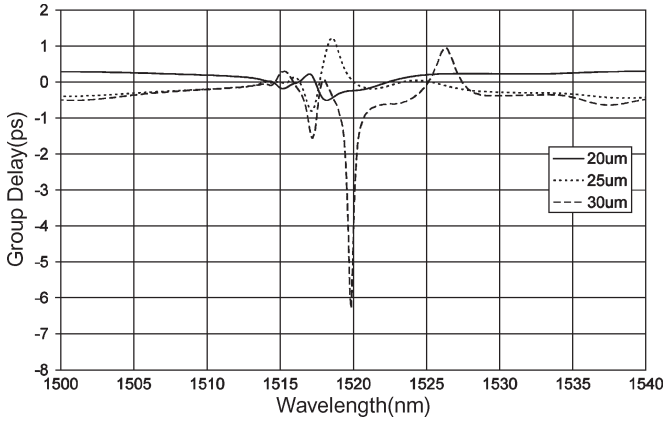

Fig. 5. GD of MSB for 20-, 25-, and 30-μm-long waveguides (different scale).

[10]. The regions of positive GD near the MSB are the slow-light regions, which are being studied for delay line and optical memory applications, and it is felt that the results and techniques that are outlined in this paper could be useful for further understanding of such devices. It can be seen that there are strong GD slopes on either side of the MSB and that pulse compression will occur in these regions. An important point to note here is that there will also be filtering effects occurring as the pulse passes through the MSB, and since the pulse is chirped, there is a potential for this to induce compression. Thus, these two effects are operating simultaneously, leading to a quite complex behavior. This paper will present results showing that the negative GD or fast-light effect plays the major role in compression in these cases.

Looking in detail at Figs. 4 and 5, it can be clearly seen that there is no simple relationship between length and GD. In fact, they show that the 10-μm-long guide gives the highest GD of all guides apart from the 30-μm-long case. It should be noted here that since the regime of operation is partly inside the MSB, the level of attenuation is an important factor to consider when designing with these types of devices. In [6], the idea of integrating the device within a gain region has been postulated, and this could reduce the impact of the MSB attenuation. Also, in a practical implementation of such a device, the weak vertical guiding structure means that the MSB region would be above the light line, which implies high losses. These losses have

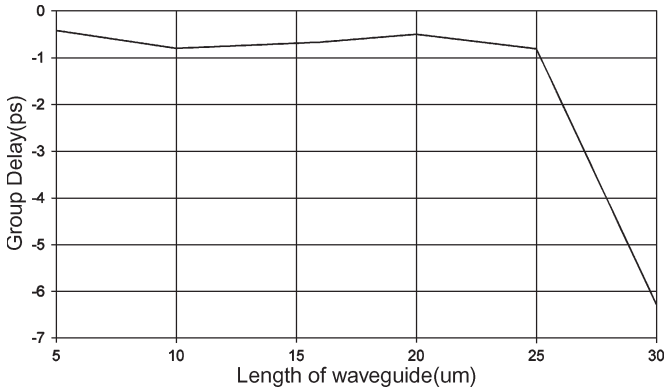

Fig. 6. Maximum GD as a function of device length taken from Figs. 3 and 4.

been studied for a number of years both in full 3-D [13], [20] and using the coupled-mode theory and measurement [9], and are typically on the order of 100–200 dB/cm. However, in the case here, the devices are very short, typically less than 30 μm, which implies losses of 0.3–0.6 dB, and it is felt that these should not have a significant impact on the overall device performance. The other important factor in these results could be the Fabry–Pérot effects occurring within the waveguide, which may have an influence on the GD response, and a detailed study of this will be the subject of future work. The results for GD are summarized in Fig. 6, where the minimum GD is plotted against the device length.

Fig. 6 highlights the very nonlinear relationship between GD and length in these short-length waveguides. It is likely that as the guides become longer, the behavior becomes more ideal as end effects reduce. However, there are many applications where short-length PhC waveguides may be of use, and these effects will be important. The GD dispersion (in picoseconds per nanometer) can be calculated by taking the derivative in Figs. 4 and 5, and this is found to have a maximum value of ± 0.5 to 2 ps/nm for all guides apart from the 30-μm-long case, which has a value of ± 15 ps/nm but only at the very high attenuation central point of the MSB. It should be noted, however, that unless the bandwidth of operation is very narrow, simple linear dispersion calculations will not apply to these types of waveguides. The results also show that the dispersion parameter D in terms of picoseconds per nanometer per millimeter becomes less meaningful since it is clear that there is no linear length dependence. This paper will proceed to show how estimates of pulse behavior can be made by combining the knowledge of the GD of an input pulse and the device GD. However, since FDTD works in the time domain, we can also observe the pulse behavior directly, and this will allow the GD-based analysis to be confirmed.

Thus, a linearly chirped pulse can be defined with a carrier wavelength close to the MSB and the output pulse observed after propagation through the PhC waveguide. A pulsewidth of 900 fs (half-width at $1/e$ intensity) is chosen since this gives a spectral width of 5.06 nm (full-width at half-maximum, FWHM), which is of the same order as the MSB width and should result in interesting behavior. Fig. 7 shows the results for this for the case of $C = 2$ for intensity normalized with respect to the input pulse. This value of chirp has been chosen since it is

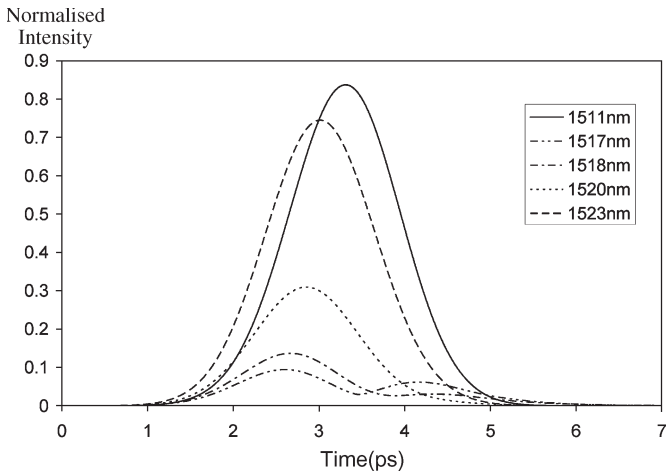

Fig. 7. Output pulses in the time domain for five different carrier wavelengths near to an MSB in the 10-μm-long waveguide for $C = 2$.

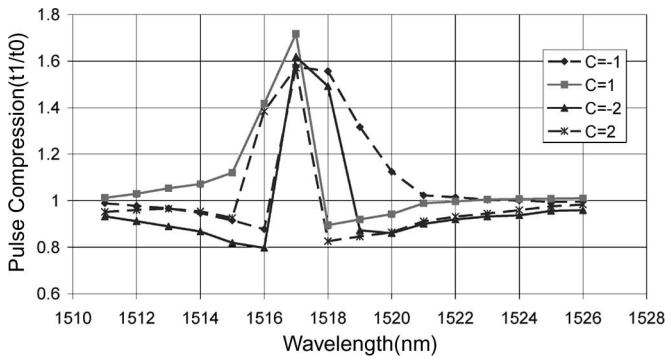

Fig. 8. Ratio of the output pulsewidth t_1 to the input pulsewidth t_0 for waveguide of Fig. 1, with $L = 10$ μm, as the carrier wavelength is swept across the MSB for different chirp values C. Compression occurs when $t_1/t_0 < 1$ (900-fs pulsewidth).

typical for devices such as semiconductor lasers and SOAs, into which it may be possible to integrate such PhC waveguides.

It can be seen that far from the MSB, the output pulses at 1511 and 1523 nm are remaining relatively unattenuated and reasonably Gaussian in shape. However, as they approach the MSB, they become more attenuated, and pulse splitting starts to occur. The compression behavior can be summarized by taking the ratio of the output pulsewidth (FWHM) to that of the input. These results are shown in Fig. 8.

Fig. 8 shows a number of interesting features, and it should be noted that each data point is derived from an 11-h FDTD simulation. Most of these results have been obtained using a high-throughput Condor [17] computing cluster containing 260 Pentium-IV processors. The cluster enables large numbers of simultaneous simulations to be run, enabling the data of Fig. 8 to be obtained reasonably easily. It is seen that pulses with both positive and negative values of C have been used, and the graphs show that the simple behavior that is predicted by (4) does not occur. That is, there is no simple relationship between expansion and compression when a sign change of C occurs. The figure shows that for $C = 1$, as the MSB is approached from the long-wavelength side, a small amount of compression starts to occur, reaching a maximum close to the center of the

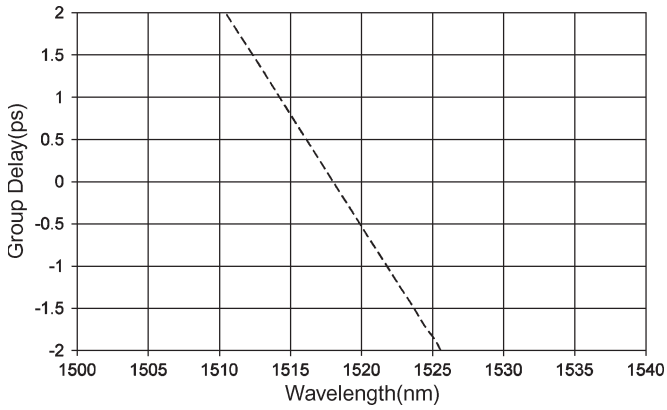

Fig. 9. GD of the input 900-fs linear chirp ($C = 2$) pulse. The carrier wavelength at the maximum pulse compression point for round holes is 1518 nm.

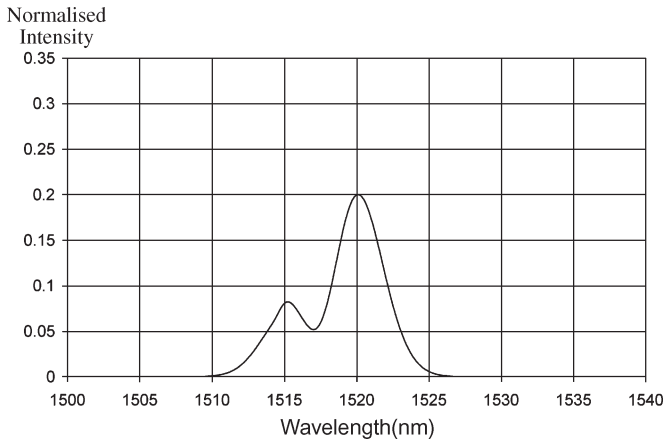

Fig. 10. Output spectrum for $C = 2$, 1518-nm pulse, through the 10-μm-long waveguide.

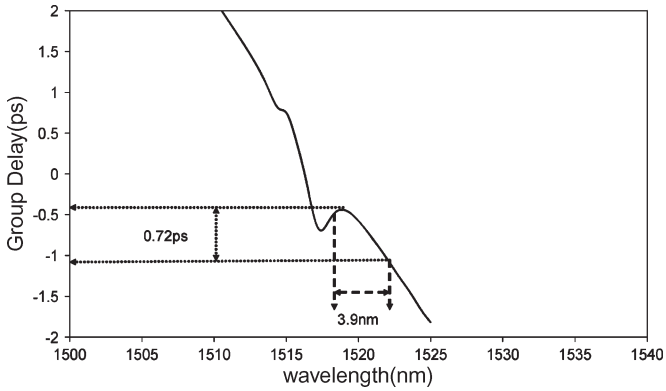

Fig. 11. Output GD for the 10-μm-long PhC waveguide for a $C = 2$ input pulse that is centered at 1518 nm.

MSB. This is followed by a rapid switch to expansion and can be seen to be due to the pulse splitting effects that occur, as shown in Fig. 7. Since a simple pulsewidth definition is being used, as soon as the secondary pulse crosses the half-power point, the output pulsewidth jumps to a high value, producing the sharp peak in Fig. 8. As the carrier wavelength continues to decrease, the expansion decreases, but it never crosses into compression. A similar behavior is seen for the case of $C = 2$, with larger compression occurring on the long-wavelength side and compression now being achieved on the short-wavelength side as well.

The GD that was derived in the first part of this section can now be used to understand all the aspects of the aforementioned behavior. To begin with, the GD of the input chirped pulse needs to be calculated. This can be derived directly from the analytic Fourier transform of (3) [14] and is shown in Fig. 9.

The GD is linear as is expected for a linear chirp, and it can been seen that in simple linear dispersion compensation, a reverse identical slope is required to correct for the dispersion. This would result in a flat GD response. This is the essence of the approach taken by this paper: We can use the flatness of the GD at the output of the PhC waveguide as an indication of how close the output pulse is to being transformed limited, i.e., at the limit of compression. As mentioned earlier for the 900-fs wide pulse with $C = \pm 2$, the transformed limited width is 402 fs; this therefore puts an upper limit on the amount of compression that can be obtained, which is 0.4466 in terms of the results in Fig. 8. Thus, to find the GD at the output, it is only required to add the GD of the pulse to the GD of the PhC waveguide. There is, however, one further requirement: To estimate the GD flatness, it is required to know the bandwidth across which to measure the flatness. This can be found from the output spectrum of the pulse. Thus, in Fig. 10, the output spectrum is shown for the case of $C = 2$ at a carrier wavelength of 1518 nm, which is the maximum compression point on the long-wavelength side of the MSB.

It can be seen that because of filtering, the maximum of the pulse spectrum is now shifted close to 1520 nm. The total GD at the output can be calculated and is plotted in Fig. 11.

The effect of the fast-light region of the MSB is clearly seen here: It reduces the GD at the short-wavelength side of the pulse and, thus, reduces the overall GD spread of the pulse. A GD flatness of 0.72 ps is obtained; it is difficult, however, in this complex dispersion environment to relate the GD flatness figure directly to the output pulsewidth, but it can be used as a figure-of-merit. The effect of filtering can also be understood from these figures. The filtering will reduce the bandwidth of the pulse and, thus, work to improve the GD flatness; however, it must be remembered that a reduction in spectral width will increase the transform-limited temporal width of the pulse. Thus, the overall effect will be reduced. This analysis can be applied on the short-wavelength side as well; Fig. 12 shows the output spectrum, and Fig. 13 shows the output GD. It can be seen that the fast-light region is now working to accelerate the long-wavelength edge of the pulse increasing the pulsewidth. Filtering effects will still occur, however, which result in the small level of compression that occurs on the short-wavelength side of between 0.9 and 1, as shown in Fig. 8. Obviously, when the sign of C changes, these same arguments apply, but swapping the short- and long-wavelength sides of the pulse. It can be seen that there is no exact symmetry when this occurs, and this is due to the unsymmetrical nature of MSBs. Thus, we have used GD to understand the complex behavior of pulses in MSBs, and this approach will be very useful in optimizing systems to achieve the best possible compression for a given pulse.

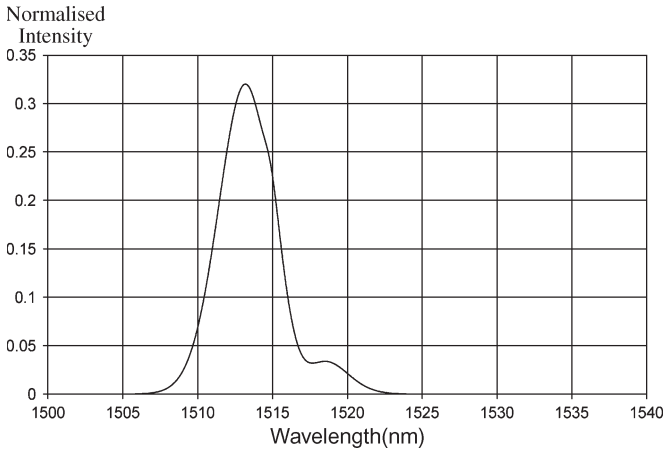

Fig. 12. Output spectrum for the 10-μm-long waveguide $(C = 2)$ that is centered at 1515 nm.

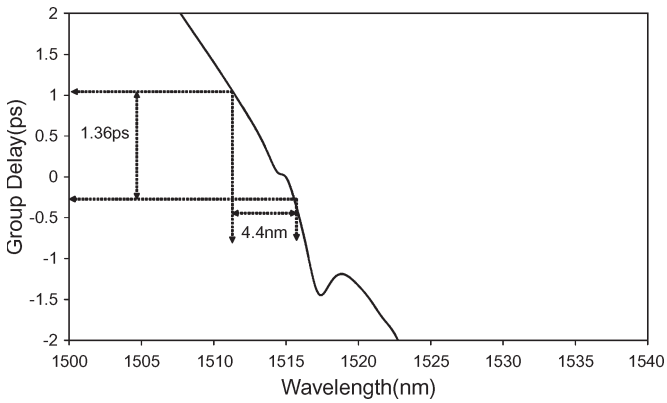

Fig. 13. Output GD for the 10-μm-long waveguide $(C = 2)$ that is centered at 1515 nm.

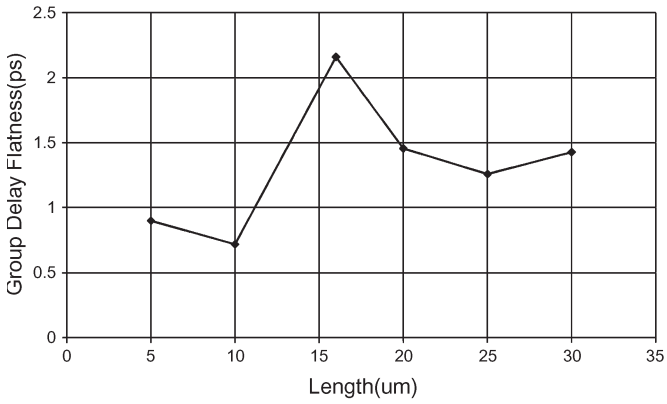

Fig. 14. Output GD flatness for different length structures.

Thus, the GD flatness figure can now be used to estimate the pulse compression performance for different length waveguides, as shown in Fig. 14. It can be seen that the 10-μm-long guide is predicted as having the best compression behavior. To confirm this, direct time-domain simulations have been carried out, and summary results are shown in Fig. 15. They confirm that, indeed, the 10-μm-long guide gives the best compression behavior. The direct time-domain results have been taken across a wide range of wavelengths, as shown in Fig. 8, and thus, the slight change in the center of the MSB with length should not effect this conclusion.

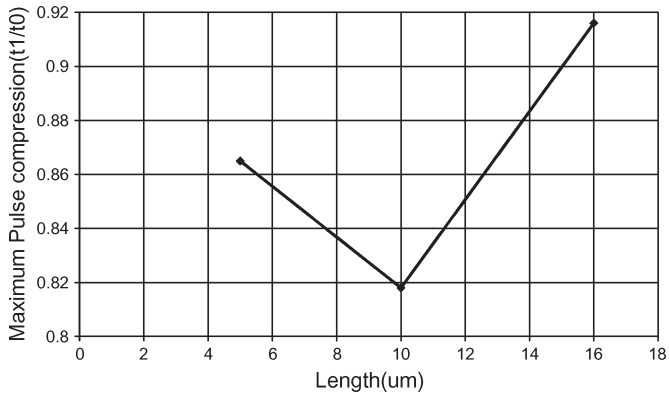

Fig. 15. Maximum pulse compression for different length structures $(C = 2)$.

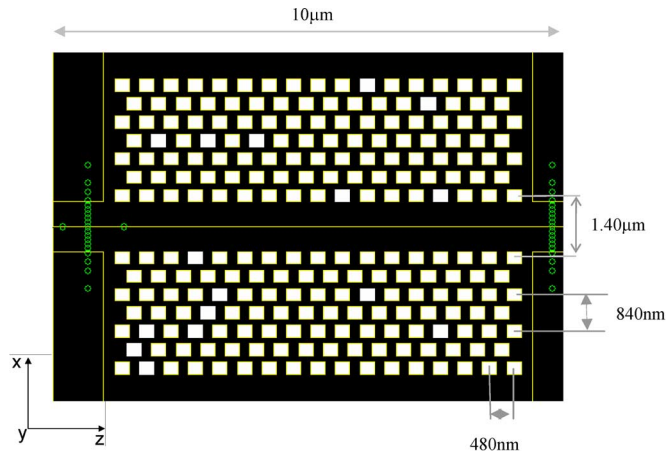

Fig. 16. FDTD model of a narrowed square-hole PhC waveguide with $a = 480$ nm, W3 guide in the $\Gamma - K$ direction, $n = 3.24$, squares holes $= 280 \times 280$ nm, and length $= 5$, 10, 16, 20, 25, and 30 μm. The FDTD mesh size in the horizontal and vertical directions is 20 nm.

Having optimized the length of the PhC waveguide, it is interesting to consider what may be the best possible compression for a given length of waveguide. To this end, a different design of waveguide was explored, with a slightly different width of 1.4 μm and using square holes. The use of nonround holes can be a fabrication challenge, but techniques such as focused-ion-beam etching [18], [19] can achieve very sharp corner features, and high-resolution E-beam systems should also be able to achieve this. Fig. 16 shows the top view the structure, and Fig. 17 shows the length dependence of the transmission through the device. In this case, an increased mesh size of 20×20 nm was used, which is sufficient to maintain a reasonable accuracy.

It can be seen that the square-hole-based waveguide has quite different and more complex transmission responses. This is due to the more complex mode coupling occurring in this case, as evidenced by the multiple MSBs that can be seen in the 10-μm-long case.

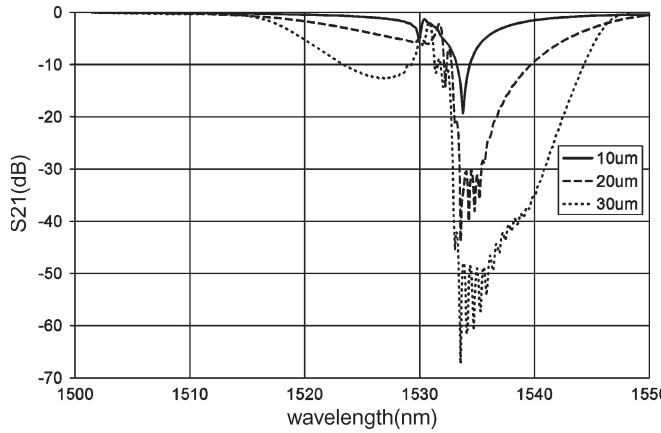

Fig. 17. FDTD simulated transmission for the 10-, 20-, and 30-μm-long waveguides of Fig. 15.

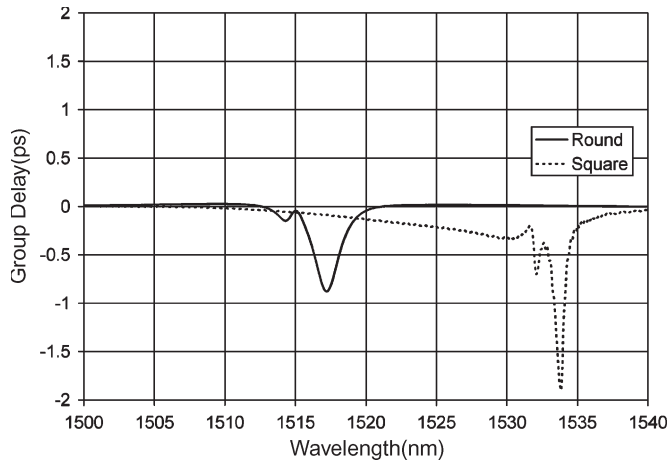

Fig. 18. GD for the 10-μm-long square-hole waveguide of Fig. 15 as compared to that for the round-hole structure.

An equivalent 1-D coupling coefficient can again be extracted using these data and (1), and a value of 0.283 μm^{-1}, which is slightly higher than that of the round-hole case, is found. Thus, one might assume that an increased GD may occur. This is plotted in Fig. 18, which shows that this is indeed the case. Thus, with an increased GD, it might be hoped that an increased compression may be achieved. Fig. 19 shows the pulse compression ratios for the square-hole case, and compression has, indeed, now increased to around 0.6, which is approaching the maximum possible in this case, i.e., 0.4466.

These direct results can again be checked using the GD flatness approach, and the output pulse GD for both round-hole and square-hole cases is shown in Fig. 20. The figure shows that as expected, the GD flatness is better in the case of the square-hole structure. Thus, this paper has shown how improved compression can be obtained by optimizing the PhC structure, albeit over quite a narrow bandwidth. Work is now on going to optimize for the maximum bandwidth as well as the maximum compression. The GD flatness approach will be used to identify what GD profile a MSB should have in order to achieve this goal.

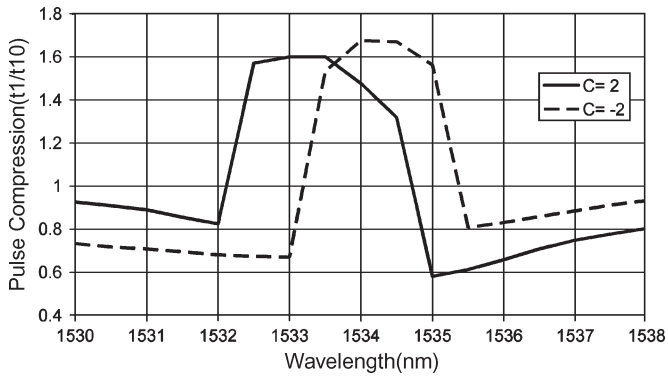

Fig. 19. Ratio of the output pulsewidth t_1 to the input pulsewidth t_0 for the 10-μm-long waveguide of Fig. 15 as carrier wavelength is swept across the MSB for different chirp values C. Compression occurs when $t_1/t_0 < 1$ (900-fs pulsewidth).

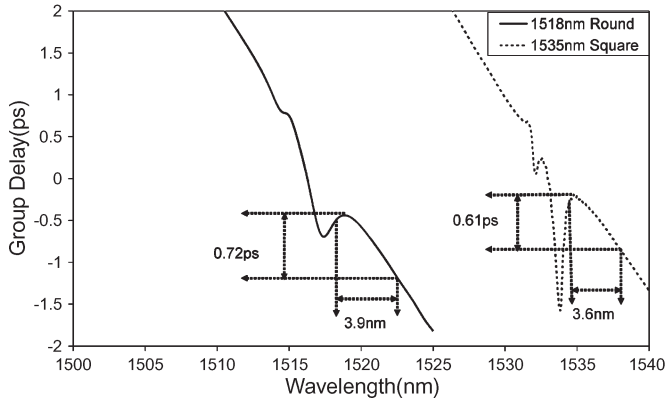

Fig. 20. Output GD for the 10-μm-long square-hole-based PhC waveguide as compared to the round-hole structure.

IV. Conclusion

This paper has studied pulse propagation in PhC waveguides using the 2-D FDTD method, both directly in the time domain and via Fourier transforms in the frequency domain, to derive the output GD response. It has been shown that there is no simple relationship between GD and length for short-length PhC waveguides when propagation is near to an MSB because of the mode coupling that is occurring. This means that the use of dispersion diagrams for pulse compressor design may not yield good results. Having calculated the GD in the frequency domain, it can be used in conjunction with the GD of an input pulse to estimate the output pulsewidth. This has been confirmed by the direct time-domain modeling, and the approach enables simple explanations of quite complex pulse behavior to be achieved. It is found that the fast-light region within the MSB plays an important role in compression and has a stronger influence than the filtering effects that are associated with the MSB. This analysis shows that ideas such as opposite edges of the MSB inducing compression and expansion, respectively, do not really apply in these complex dispersion and filtering environments. Since the pulse is partially inside an MSB, care must be taken not to attenuate the pulse too greatly. It is hoped that combining the approach with a gain medium may overcome this limitation. This paper then studies the length dependence

of the pulse compression, and it is found that the GD flatness and direct time-domain simulation both agree that, in this case, 10 μm is the optimum length. Finally, the optimum compression for a given length is studied, and a square-hole-based design is shown to have an increased compression in agreement with the GD flatness analysis. This simplified analysis will enable the optimum MSB GD profile to be determined, which can then be used to drive an optimization process to find the required PhC waveguide design to achieve this. It is hoped that tunable designs can be achieved, which may even be able to perform a real-time control of dispersion in the next-generation high-speed optical communications systems.

ACKNOWLEDGMENT

The authors would like to thank Prof. J. McGeehan for the use of the Condor computing cluster, which was donated to Bristol Electrical and Electronic Engineering by Toshiba Research Laboratories Europe, and P. Wade and P. Townsend for implementing and maintaining the cluster.

REFERENCES

[1] M. Notomi *et al.*, "Extremely large group-velocity dispersion of line-defect waveguides in photonic crystal slabs," *Phys. Rev. Lett.*, vol. 87, no. 25, p. 253 902, Dec. 2001.

[2] T. J. Karle *et al.*, "Observation of pulse compression in photonic crystal coupled cavity waveguides," *J. Lightw. Technol.*, vol. 22, no. 2, pp. 514–519, Feb. 2004.

[3] A. Y. Petrov and M. Eich, "Dispersion compensation with photonic crystal line-defect waveguides," *IEEE J. Sel. Areas Commun.*, vol. 23, no. 7, pp. 1396–1401, Jul. 2005.

[4] A. Xing, M. Davanço, S. Camatel, D. J. Blumenthal, and E. L. Hu, "Pulse compression in line defect photonic waveguide," presented at the Optical Fiber Commun. Conf., Anaheim, CA, 2005, Paper OWD5.

[5] M. Davanço, A. Xing, J. Raring, E. L. Hu, and D. J. Blumenthal, "Detailed characterization of slow and dispersive propagation near a mini-stop-band of an InP photonic crystal waveguide," *Opt. Express*, vol. 13, no. 13, pp. 4931–4938, Jun. 27, 2005.

[6] T. Cao, M. J. Cryan, I. J. Craddock, J.-Z. Zhang, I. Galbraith, T. Karle, S. Yu, J. Rorison, and C. J. Railton, "Modelling of a 2D photonic crystal waveguide pulse reshaper integrated with a SOA," in *Proc. CLEO Europe*, Munich, Germany, Jun. 2005, p. 606.

[7] L. A. Coldren and S. W. Corzine, *Diode Lasers and Photonic Integrated Circuits*. Hoboken, NJ: Wiley, 1995.

[8] J. Zhao, "An object-oriented simulation program for fibre Bragg gratings," M.S. thesis, Rand Afrikaans Univ., Johannesburg, South Africa, Oct. 2001.

[9] S. Olivier, H. Benisty, C. Weisbuch, C. J. M. Smith, T. F. Krauss, and R. Houdré, "Coupled-mode theory and propagation losses in photonic crystal waveguides," *Opt. Express*, vol. 11, no. 13, pp. 1490–1496, Jun. 2003.

[10] S. Longhi, M. Marano, M. Belmonte, and P. Laporta, "Superluminal pulse propagation in linear and nonlinear photonic grating structures," *IEEE J. Sel. Topics Quantum Electron.*, vol. 9, no. 1, pp. 4–16, Jan./Feb. 2003.

[11] A. Taflove and S. C. Hagness, *Computational Electrodynamics: The Finite-Difference Time-Domain Method*. Norwood, MA: Artech House, 2005.

[12] I. J. Craddock *et al.*, "Applications of single mode extraction from finite difference time domain data," *Proc. Inst. Electr. Eng.—Microw. Antennas Propag.*, vol. 146, no. 2, pp. 160–162, Apr. 1999.

[13] M. J. Cryan, D. C. L. Wong, I. J. Craddock, S. Yu, J. Rorison, and C. J. Railton, "Calculation of losses in 2D photonic crystal membrane waveguides using the 3D FDTD method," *IEEE Photon. Technol. Lett.*, vol. 17, no. 1, pp. 58–60, Jan. 2005.

[14] G. P. Agrawal, *Fiber-Optic Communication Systems*. Hoboken, NJ: Wiley, 1992.

[15] M. J. Cryan *et al.*, "Design and simulation of a photonic crystal waveguide filter using the FDTD method," in *Proc. IEEE LEOS*, Glasgow, U.K., Nov. 2002, pp. 516–517.

[16] C. K. Madsen and J. H. Zhao, *Optical Filter Design and Analysis: A Signal Processing Approach*. New York: Wiley, 1999.

[17] [Online]. Available: http://www.cs.wisc.edu/condor/

[18] C. G. Bostan *et al.*, "Line-defect waveguides in hexagon-hole type photonic crystal slabs: Design and fabrication using focused ion beam technology," in *Proc. IEEE LEOS Benelux Meeting*, 2003, pp. 253–256.

[19] K. Balasubramanian, P. J. Heard, and M. J. Cryan, "Focused ion beam fabrication of 2D photonic crystals in silicon-on-insulator," *J. Vac. Sci. Technol. B, Microelectron. Process. Phenom.*, vol. 24, no. 6, pp. 2533–2537, Nov./Dec. 2006.

[20] M. J. Cryan, I. J. Craddock, S. Yu, C. J. Railton, and J. Rorison, "Analysis of losses in 2D photonic crystal waveguides using the 3D finite difference time domain (FDTD) method," in *Proc. IEEE LEOS*, Glasgow, U.K., Nov. 2002, pp. 516–517.

Tun Cao was born in Dalian, China, in 1979. He received the B.Eng. degree in electronic engineering and the B.Eng. degree in computer science from Dalian University of Technology, Dalian, in 2001 and 2002, respectively, and the Ph.D. degree from the University of Bristol, Bristol, U.K., where his doctoral research focused on FDTD and finite-element analysis of photonic crystals, focus-ion-beam fabrication, and measurement of nanophotonic devices.

He is currently with the Detectors and Nuclear Science Research Group, Institute of Health Sciences, City University, Northampton Square, London, U.K.

Martin J. Cryan (S'91–M'95–SM'01) received the B.Eng. degree in electronic engineering from the University of Leeds, Leeds, U.K., in 1986 and the Ph.D. degree from the University of Bath, Bath, U.K., in 1995.

He worked in industry for five years as a Microwave Design Engineer in 1986. From 1994 to 1997, he was a Researcher with the University of Birmingham, Birmingham, U.K., where he worked on active integrated antennas. From 1997 to 1999, he was a European Union Training and Mobility of Researchers Research Fellow with the University of Perugia, Perugia, Italy, where he worked on the design and simulation of quasi-optical multipliers using the lumped-element FDTD method. From 2000 to 2002, he was a Research Associate with the University of Bristol, Bristol, U.K., where he worked on hybrid electromagnetic methods for EMC problems in optical transceivers and FDTD analysis of photonic crystals. He is currently a Senior Lecturer with the Department of Electrical and Electronic Engineering, University of Bristol. He has published 24 journal and 74 conference proceedings (including seven invited) on fabrication, modeling, and measurement of photonic-crystal-based devices, RF over fiber, active integrated antennas, FDTD analysis, and MMIC design.

Ying-Lung Daniel Ho received the B.Sc. degree in electrical engineering from the National Taipei University of Technology, Taipei, Taiwan, R.O.C., in 1999 and the Ph.D. degree from the University of Bristol, Bristol, U.K., in 2007.

He is currently a Postdoctoral Researcher with the Photonics Research Group, Centre for Communications Research, Department of Electrical and Electronic Engineering, University of Bristol. His current research interests include FDTD modeling and simulation of quantum optics in wavelength-scale structures, and focused-ion-beam fabrication of microoptical/nanooptical devices, including semiconductor and diamond-based single-photon sources.

Ian J. Craddock received the B.Eng. and Ph.D. degrees from the University of Bristol, Bristol, U.K., in 1992 and 1995, respectively.

He is a Reader in the Centre for Communications Research, Department of Electrical and Electronic Engineering, University of Bristol. He has active research interests in FDTD, wide-band antenna design, antenna arrays, MIMO, electromagnetic analysis, and microwave radar for breast cancer detection. He is part of the EU Framework 6 Antennas Network of Excellence, where he leads a workpackage on antennas for GPR.

Chris J. Railton received the B.Sc. degree in physics with electronics from the University of London, London, U.K., in 1974 and the Ph.D. degree in electronic engineering from the University of Bath, Bath, U.K., in 1988.

From 1974 to 1984, he worked with the scientific civil service on a number of research and development projects in the areas of communications, signal processing, and electromagnetic compatibility. From 1984 to 1987, he was with the University of Bath, working on the mathematical modeling of boxed microstrip circuits. He is currently leading the Computational Electromagnetics Group, Centre for Communications Research, Department of Electrical and Electronic Engineering, University of Bristol, Bristol, U.K. He has worked on many different electromagnetic analysis methods, in particular, the finite-difference time-domain method, for over two decades, where he has pioneered a number of new techniques to advance the state of the art. In addition, he has been active in other modeling techniques, particularly the spectral domain method and partial-element equivalent circuits, and in the development of hybrids consisting of electromagnetic, thermal, and semiconductor models. He has published in more than 90 journal and conference proceedings in this area and has been an invited speaker at a number of international electromagnetics conferences.